ADVANCED MATERIALS TECHNOLOGIES

www.advmattechnol.de

Liquid Metal-Conductive Thermoplastic Elastomer Integration for Low-Voltage Stiffness Tuning

Steven Rich, Sung-Hwan Jang, Yong-Lae Park, and Carmel Majidi*

An electrically responsive composite is introduced that exhibits muscle-like changes in elastic stiffness (≈1–10 MPa) when stimulated with moderate voltages (5–20 V). The stiffness-tuning element contains an embedded layer of conductive thermoplastic elastomer (cTPE), composed of a propylene–ethylene copolymer and a percolating network of carbon black. Two opposite surfaces of the cTPE layer are coated with a ≈20 μm thin film eutectic gallium–indium (EGaIn) liquid metal alloy. When a voltage is applied to these EGaIn electrodes, electric current passes through the cTPE. This causes internal Joule heating, which induces a phase transition that changes the composite from its stiff state (E = 10.4 MPa) to its compliant state (E = 0.7 MPa). Differential scanning calorimetry is performed to show that this state change is governed by a solid–liquid transition. Voltage-dependent activation times are demonstrated that can be reduced to below 2 s and show the ability of the composite to recover its original shape after large strains. To illustrate its applicability in robotics, the composite is incorporated into an underactuated robotic finger, providing it with two different bending modes. The ability to use the composite as a moldable stiffness-tuning splint is also demonstrated.

The ability to tune elastic rigidity – i.e., change between a soft, flexible state, and a stiffer, more rigid state – is critical to many biological systems such as natural muscle,[1] hydrostatic skeletons (e.g., limbs of cephalopods),[2] and catch connective tissue (found in sea cucumbers and other echinoderms).[3] These systems enable the load-bearing functionality of rigid structures, while maintaining the compliance and adaptability of soft morphologies.[4] Their capacity to rapidly, dramatically, and reversibly change rigidity is also attractive for artificial muscle actuators,[5,6] which are becoming increasingly suitable for wearable devices. The goal of rigidity tuning has been addressed using methods like solvent interactions,[7] pneumatic jamming,[8,9] electrostatic adhesion,[10] antagonistic actuator architectures,[11–13] fluidic flexible matrix composites,[14] phase-change materials,[15–27] and magnetorheological fluids.[28] The diversity of these methods results in an equally diverse range of technical challenges, such as long activation times, high activation voltages,[10,15] limited scalability and structural versatility,[11–13,26,27] and a dependence on bulky auxiliary equipment.[8,9,14,17,28] At present, there remains to be an electrically powered method for reversible rigidity tuning that exhibits <5 s, <20 V, actuation in a size-scalable architecture that allows for integration into a wide range of systems.

In this work, we introduce a rigidity-tuning material architecture that changes stiffness in response to moderate electrical voltage (**Figure 1**a,b and Video S1 (Supporting Information)). Furthermore, we demonstrate its feasibility in both tensile and flexural applications, via an active tendon in an underactuated robotic finger model[29] and a moldable splint (Figure 1c,d). The tendon consists of a conductive thermoplastic elastomer (cTPE) coated with a ≈10–140 μm layer of spray-deposited eutectic gallium–indium liquid metal alloy (EGaIn)[30] and embedded in a silicone matrix (Figure 1b). Applying voltage to the EGaIn electrodes causes electric current to travel through the cTPE element. This induces rapid Joule heating in the cTPE, bringing it to the melting temperature, above which it softens and can no longer support a tensile load. When current is removed, the element cools and solidifies, and its stiffness is restored. Previously, shape memory polymers (SMPs)[16,18–20,23–25,31] and low-melting-point alloys[20–22,26,27,32] have also been incorporated into reversible, stiffness-based adhesives and rigidity-tuning elements. Although some of these methods may have very large stiffness change ratios, they typically require external heating equipment or long activation times (**Table 1**). Shan et al. exploited Joule heating to directly electrically activate cTPE; however, this technique required activation voltages of above 100 V.[15]

We build on previous work with cTPE by introducing a novel design, in which a pair of liquid metal electrodes is oriented on opposite sides of the cTPE. This configuration minimizes the

S. Rich, Prof. C. Majidi
Department of Mechanical Engineering
Carnegie Mellon University
Pittsburgh, PA 15213, USA
E-mail: srich@andrew.cmu.edu
Dr. S. H. Jang
Civil and Coastal Engineering
Plymouth University
Plymouth PL4 8AA, UK
Prof. Y. L. Park, Prof. C. Majidi
Robotics Institute
Carnegie Mellon University
Pittsburgh, PA 15213, USA
Prof. Y. L. Park
Department of Mechanical and Aerospace Engineering
Seoul National University
Seoul 151–742, South Korea

DOI: 10.1002/admt.201700179

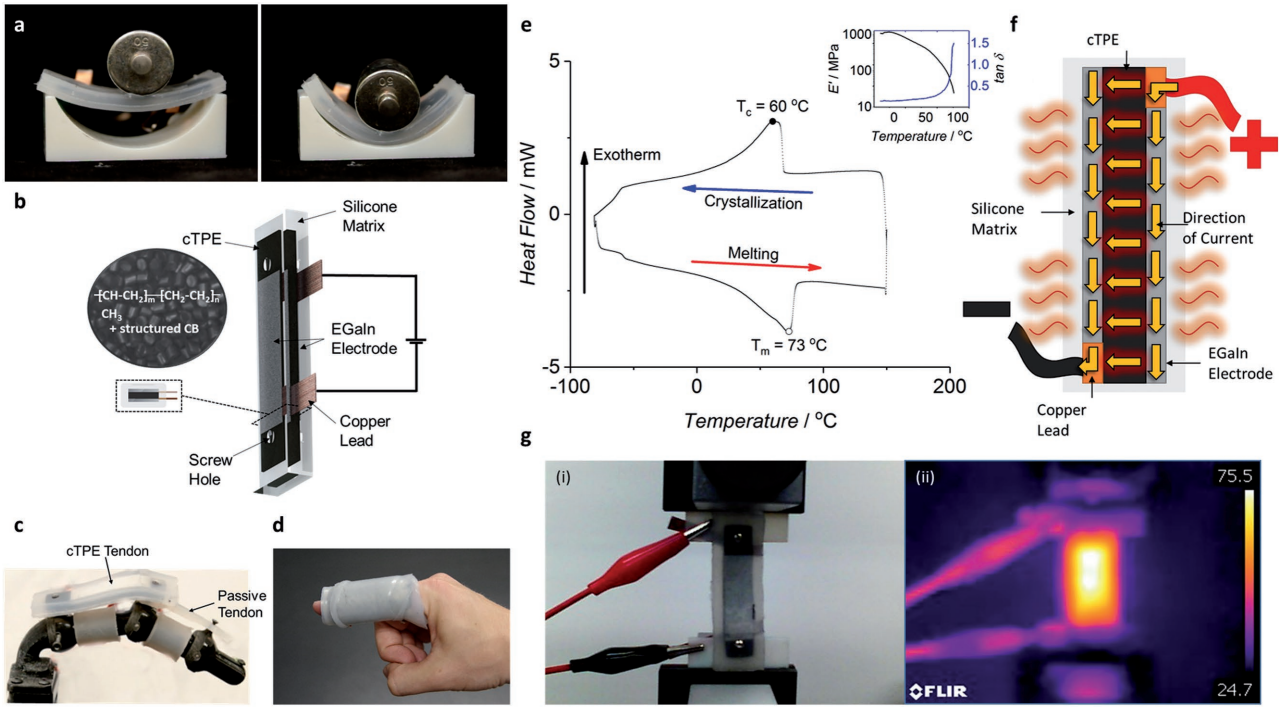

Figure 1. Tendon composition and implementation. a) The unactivated and activated tendon's response to a 50 g mass applied to its center. The stiffness of the unactivated tendon is higher than 10 MPa, while the stiffness of the actuated tendon is less than 1 MPa, resulting in the bending of the activated tendon in response to the mass. b) The layup of the tendon. A 1 mm layer of cTPE is impressed with copper leads on opposite sides and coated with a spray-deposited layer of EGaIn. This element is embedded in a silicone elastomer matrix for mechanical and electrical stability. Screw holes provide a secure attachment location for testing and implementation. The two insets show the composition of the cTPE and the cross-section of the tendon layup. c) Integration of the active cTPE tendon into a robotic finger with two activation modes, showing the cTPE in tensile applications. d) Integration of an active cTPE sheet into a moldable splint, showing the cTPE in flexural applications. e) Differential scanning calorimetry plot of conductive thermoplastic elastomer (cTPE) between –80 and 150 °C. This plot shows the second heating cycle with the exothermic direction oriented upward. The first cycle shows some abnormalities due to thermal stresses, but in cycles 2–4, the behavior converges. The peak at 73 °C indicates the melting temperature (T_m), while the peak at 60 °C represents the crystallization temperature (T_c). The kink between –80 and –50 °C represents the glass transition temperature; however, this value cannot be determined without examining the heat flow at lower temperatures. The inset shows DMA data, which corroborate the softening temperature found in the DSC data. f) Depiction of current direction during activation. The current flows along the lower resistance liquid metal electrodes, and then passes through the thickness of the cTPE. The current results in significant Joule heating in the cTPE, which eventually heats the whole architecture and is dissipated into the surroundings. g) Configuration and temperature response of the tendon during activation. (i) is a visible light photo of the tensile testing set-up during activation, and (ii) is an infrared photo, taken simultaneously from a distance of 10 mm (C2, FLIR). There is even heating across the tendon above the activation temperature.

electrical resistance of the actuator by minimizing distance that current must travel through the percolating network of carbon black, allowing for lower voltages (5–20 V), faster activation times (1–40 s), and more versatile activation geometries. These improvements expand the capabilities and possible utilities of rigidity tuning elements in robotics and wearable technologies.

Table 1. Comparison between thermally activated stiffness-tuning methods demonstrated in recent studies. Acronyms: cTPE = conductive thermoplastic elastomer, LMPA = low-melting-point alloy, TP = thermoplastic, SMP = shape-memory polymer.

Author (year)	Activation time [s]	Voltage [V]	Stiffness ratio	Material
Current work	2–40	5–20	15	cTPE
Tonazzini et al. (2016)[21]	29	External heating	700	LMPA
Van Meerbeek et al. (2016)[22]	Not reported	External heating	18	LMPA
Zheng et al. (2015)[27]	6–160	4–5	Not reported	LMPA
Shan et al. (2015)[15]	6	100	25	cTPE
Balasubramanian et al. (2014)[16]	2.4	External heating	76	TP
Schubert et al. (2013)[26]	1	Not reported	27	LMPA
Shan et al. (2013)[20]	130	0.6	9033	LMPA
McKnight et al. (2010)[18]	>60	Not reported	77	SMP

We begin by performing thermoanalytical testing to determine the activation mechanism for material softening. This is followed by electromechanical testing, which is performed to establish the influence of voltage on activation time and stiffness. The results from these measurements are important for establishing a semiempirical model that can inform tendon design in potential applications. By determining the relevant material parameters and coupling laws, we enable the application-specific design of cTPE–EGaIn-based stiffness-tuning components.

The cTPE is composed of a copolymer of polypropylene (PP) and polyethylene (PE) and a percolating dispersion of structured carbon black (weight composition: 51%/9%/40%). Because of the high concentration of carbon black (CB), the entire elastomer exhibits mesoscale conductivity through percolation and electric tunneling between CB aggregates.[33] Differential scanning calorimetry (DSC) is performed on an 8.8 mg sample. Referring to Figure 1e, the cTPE shows a glass transition below −60 °C, a melting peak at 72.9 ± 0.07 °C, and a crystallization peak at 59.8 ± 0.07 °C. This suggests that electrically induced cTPE softening is caused by a solid–liquid phase transition rather than a glass transition or Vicat softening, as previously claimed for a PE–PP–CB composition.[15] Such results are consistent with measurements obtained using dynamical mechanical analysis (DMA), which is shown in the inset of Figure 1e. As expected, we observe a significant drop in storage modulus and a peak in damping factor as the temperature exceeds 75.0 °C. Above this temperature, the storage modulus is approximately one order of magnitude smaller than that measured at room temperature. Although the addition of fillers such as carbon black may slightly change the thermal properties of the host matrix material, the values found in the DSC and DMA measurements resemble those of the unfilled propylene–ethylene copolymer.[34] We note that the DSC plot shows a melting peak offset 13 °C higher than crystallization peak, revealing some thermal hysteresis in the material. The lower crystallization temperature indicates a potential delay in the restiffening response when integrated in the tendon architecture.

In order to reach the activation temperature, T_a, the cTPE functions as a Joule heater, transforming electrical energy to heat (Figure 1f). The effect of this heating can be seen in the infrared photograph in Figure 1g. This process can be described using conservation of energy

$$E_i = E_{st} + E_o \tag{1}$$

where E_i is the electrical energy input, E_{st} is the energy stored within the tendon, and E_o is the energy released. To find the E_i required to induce phase change, we examine the components of the right side of the equation. Since heat is dissipated from the surface of the tendon by convection and radiation (conduction is neglected, since the tendon is attached to the test set-up at the unactivated screw holes), the energy released can be expressed as $E_o = \Delta H_{conv} + \Delta H_{rad}$, where ΔH_{conv} is the heat lost to convection, and can be rewritten as $\Delta H_{conv} = \int_0^{t_a} q\,dt = \int_0^{t_a} hA(T_s - T_\infty)dt$, and ΔH_{rad} is the heat lost to radiation, given by $\Delta H_{rad} = \int_0^{t_a} q\,dt = \int_0^{t_a} \varepsilon\sigma A T_s^4\,dt$.

In these equations, t_a is the activation time, q is the heat transfer rate, h is the heat transfer coefficient, A is the area of the tendon, T_s is the surface temperature of the tendon as a function of time, T_∞ is the ambient temperature, ε is the emissivity, and σ is the Stefan–Boltzmann constant.

The stored energy, E_{st}, is composed of the change in enthalpy of the cTPE required to induce melting from room temperature (ΔH_a) and the heat stored in the surrounding silicone matrix (ΔH_{sil}). We can find ΔH_a by integrating the area beneath the melting peak of the DSC plot (located in the lower half of the heating loop) and dividing by the heating/cooling rate (Figure 1e), while ΔH_{sil} can be expressed by $\Delta H_{sil} = \rho V C_p(T_f - T_\infty)$, where ρ is the density of the silicone, V is the volume, T_f is the final temperature, and C_p is its specific heat capacity. Thus, we see that the electrical energy required for activation, E_i, can be calculated by summing the required heat for melting the cTPE, the heat stored in the silicone matrix, and the losses due to conduction and convection

$$E_i = \Delta H_a + \rho V C_p(T_f - T_\infty) + \int_0^{t_a} [hA(T_s - T_\infty) + \varepsilon\sigma A T_s^4]\,dt \tag{2}$$

We can then balance this prescribed energy for activation, E_i, with the expression for electrical energy input, given by the integral of the power input curve (Figure S1, Supporting Information), yielding

$$E_i = \int_0^{t_a} VI\,dt = \int_0^{t_a} \frac{V^2}{R}dt \tag{3}$$

The right side of Equation (3) represents the scaling law that shows that for a prescribed energy input, E_i, minimizing the tendon resistance R can permit low-voltage activation, achievable with a 9 V battery. We also see that longer activation times lead to greater losses from increased convection and radiation, which are somewhat underpredicted by these equations (see Table S1 in the Supporting Information for calculations).

To achieve activation with low-to-moderate voltages, we minimize the electrical resistance of the tendon by providing electrical current through electrodes situated across the thickness of the cTPE (Figure 1b). This reduces the conducting length and maximizes the cross-sectional area, yielding a total resistance for the system that is less than 1 Ω. Under 5 V, the tendon can reach an activation temperature, T_a, defined as the melting temperature, in ≈40 s. Although the cTPE shows considerable softening when temperatures are elevated but still below T_a, the response stabilizes after the sample fully melts, yielding distinct activated and unactivated states (**Figure 2**a). Since the modulus approaches an asymptote as temperature rises, we define the activation time, t_a, as the time for the modulus to drop by 90% of its total decrease, when starting from room temperature (Figure 2b). Both t_a and the maximum temperature achieved are highly dependent on the voltage applied across the tendon, since the energy input to the system rises with the square of voltage (Equation (3)). By raising this value up to 20 V, we can achieve activation within 2 s (Figure 2c).

Since the electrical resistance of the tendon is dependent on both the material and mechanical properties of the sample, the

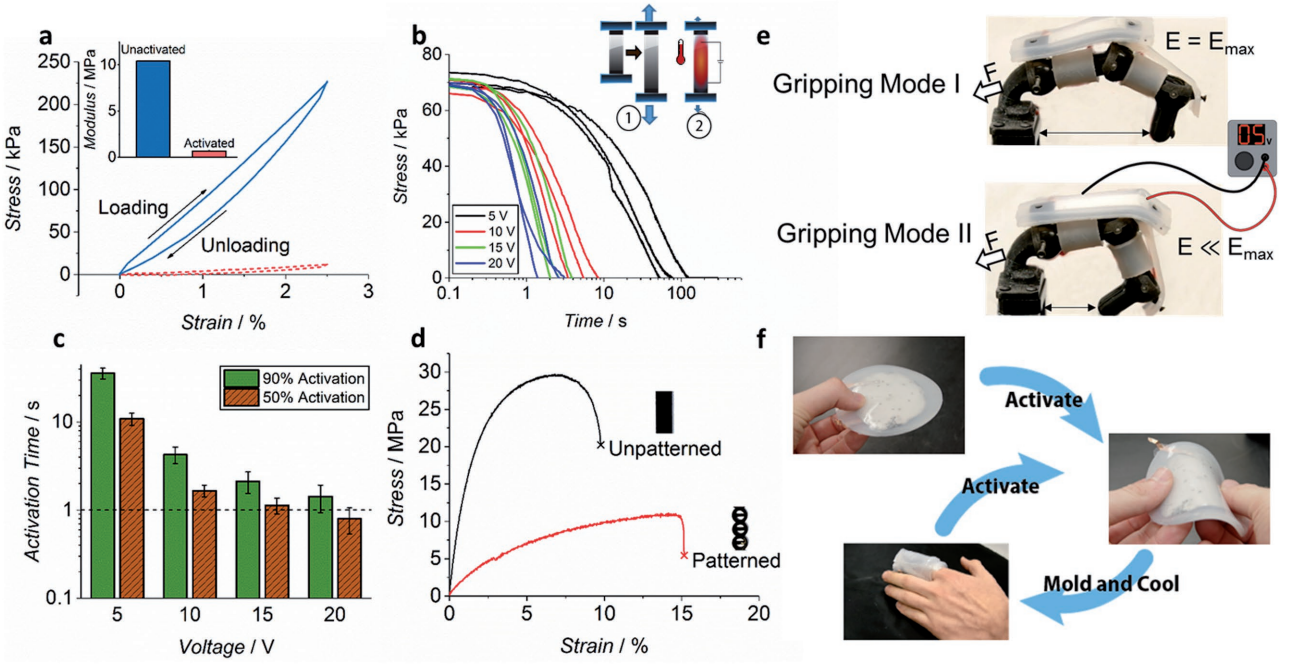

Figure 2. Stress response of the activated and unactivated tendons. a) Stress–strain plot for the extension and contraction of the tendon in the unactivated (stiff) and activated (soft) states between 0% and 2.5% strain at 0.5 mm s^{-1}. The maximum modulus is 10.4 ± 0.5 MPa, while the minimum modulus is 0.7 ± 0.08 MPa. There is a small degree of hysteresis in both states. b) ① shows that a stress of ≈70 kPa is applied to the tendon, resulting in a small strain. In ②, a voltage is applied, resulting in the heating and softening of the tendon. The resulting stress response as a function of time is shown when activated with various voltages. Higher voltages result in a faster drop in applied stress, with the highest voltages showing a significant drop in stress in less than a second. c) The activation time for tendon samples under various applied voltages, when activation is considered as 90% of the maximum drop in modulus (green) or 50% of the maximum drop in modulus (brown). d) The stress strain behavior of unpatterned and patterned cTPE tendons, demonstrating the potential for tuning the preactivation stiffness. e) An underactuated robotic finger with two gripping modes, enabled by an active cTPE tendon. A string attaches to the fingertip and provides activation force. When this string is pulled, the finger bends at the distal joint when the cTPE tendon is unactivated, and at both the distal and proximal joint when the cTPE tendon is activated. f) A voltage-activated moldable splint, enabled by a cTPE sheet. Activating the sheet with electric current renders it soft and moldable across its entire surface area, which allows it to conform to the hand. Removing the electric current causes it to harden in this new position, providing support to the target joint.

resistance and therefore the heating rate change with both its temperature and deformation. As the temperature rises, the cTPE increases in resistance, due in part to the thermal expansion of the polymer, which increases the length of the percolating pathways between carbon black particles, and thus the resistivity of the cTPE.[35] This added resistance reduces the current through the cTPE and creates a stabilizing negative feedback loop. However, as the deformation increases the current, the heating rate increases dramatically, which could be due to a decrease in conducting length from the Poisson effect (Figure S2, Supporting Information). When the temperature rises significantly above T_a, the cTPE is at risk for thermal damage. In future work, a thermocouple could provide feedback for control that would limit the maximum temperature to just above T_a. Although the cTPE in the melted state experiences inelastic deformation when the tendon is extended, the silicone matrix provides sufficient restoring force to return the tendon to its original state. Experiments to determine the ability of the matrix to regulate the shape of the tendon are performed. Even at large deflections, the tendon exhibits only a small change in its natural length and shows similar behavior to stress–strain curves at smaller strain values (Figure S3, Supporting Information). Similarly, viscoelastic effects (Figure S4, Supporting Information) and strain cycling effects (Figure S5, Supporting Information) are shown to be negligible in the activated tendons. We also demonstrate the control that patterning provides over the elastic properties of the tendon (Figure 2d), which increases the range of its potential applications.

The functionality of these cTPE tendons is demonstrated with two illustrative use cases. In the first demonstration, the cTPE is incorporated into an articulated finger model as an active tendon (Figure 2e and Video S2 (Supporting Information)), giving the finger two bending modes with a single actuator. When the tendon is unactivated, the stiffness at the proximal cTPE tendon is an order of magnitude higher than that at the purely silicone distal tendon, preventing bending at the proximal joint. Thus, pulling the string connected to the tip of the finger results in bending at only the distal joint. When the tendon is activated under 5 V, the stiffness of the proximal tendon is similar to that of the pure silicone tendon, resulting in bending at both joints when tension is applied to the string. In this way, different gripping motions, such as precision and power grips, can be achieved with only a single actuator for the multijoint finger simplifying not only the mechanical system but also the actuation mechanism.

We also show the versatility of this cTPE layup for wearable medical applications. Splints are widely used to treat conditions that require joint immobilization, such as osteoarthritis

or ulnar collateral ligament tears.[36] For decades, they have often incorporated thermoplastics to enable the patient to conform the splint to their body and reshape it if they experience discomfort.[37] Applying the heat necessary to soften the thermoplastics, however, requires bulky or specialized equipment like heat guns or water baths that make on-the-go adjustments impractical. To provide portable, reversible stiffness tuning, we incorporate a cTPE sheet into a moldable stiffness-tuning splint (Figure 2f and Video S3 (Supporting Information)). Previous direct heating stiffness-tuning methods[15,20] had active geometries restricted to the shortest linear path between the two electrodes, making it difficult to tune the stiffness of active sheets. By orienting the electrodes across the full face of the cTPE, we make the full surface area the shortest path between the electrodes, allowing us to activate any arbitrary cTPE geometry. When voltage is applied across the two electrodes, the cTPE sheet heats up and melts, transitioning from a stiff, elastic state to a soft, moldable state that is capable of conforming to a patient's hand. A silicone wrap helps to secure the compliant sheet and ensure its proper configuration. Once the cTPE sheet has been applied to the target area, the voltage is removed and the sheet returns to its stiff state, functioning as a splint. Although the cTPE must reach 70 °C for activation, it is insulated from the skin with a layer of stretchable nylon fabric.

In summary, we integrate liquid metal electrodes and a cTPE to create a low-voltage, reversible, stiffness-tuning tendon in wearable and underactuated applications. When a voltage is applied to the electrodes, the cTPE layer undergoes Joule heating and mechanically softens. This transition gives the tendon two states: a rigid state with modulus $E = 10.4 \pm 0.5$ MPa and a soft state with modulus 0.7 ± 0.08 MPa. DSC and DMA measurements performed on an isolated cTPE sample suggest that the softening is governed by a liquid–solid phase transition. By arranging the electrodes to minimize the effective resistance of the actuator, the required voltage for activation (5 V) and minimum activation time (<2 s) have been significantly reduced. Furthermore, this new configuration enables a variety of new geometries for directly activated materials, which were unattainable by previous methods. The ability of the tendon to retain its original shape after activation and significant strains is also demonstrated. Finally, we present two demonstrations of the functionality of the rigidity-tuning element: an active tendon in an underactuated finger, and a moldable stiffness-tuning splint. Future work includes incorporating temperature control into the embedding layer to ensure that the stiffness-tuning element does not heat to temperatures that may damage the tendon or become uncomfortable for the user.

Experimental Section

The cTPE sheets which formed the stiffness-tuning elements of the tendons were formed by compressing conductive polymer pellets (THEMIX Plastics Inc.) at a temperature of 160 °C to a thickness of 1.1 mm using a hydraulic heat press (Model C 3912, Carver). They were cut into strips of 5 cm × 1 cm using a 30 W CO_2 laser (VLS 3.50, Universal Laser Systems). These strips were embedded with copper leads using the heat press with the same settings as above. EGaIn (Rotometals) was deposited on both sides of the strips using a spray gun (40 psi, with Ar gas as a carrier), avoiding the portions of the mechanical and electrical contacts where actuation was not desired (Figure 1b). The tendons were symmetrically embedded into a 3 mm matrix of silicone (Ecoflex 00-30, Smooth-On): a lower layer of silicone was cured in a mold printed from an 3D printer (Objet 24, Stratsys), the EGaIn-painted cTPE was aligned with the embedding layer, and a secondary mold was screwed onto the base mold that allowed another layer of silicone to be poured over top. All samples were degassed and cured in an oven at 80 °C.

In order to activate the tendons, alligator clips were attached to the copper leads and a voltage was applied using a power supply (Model Digi 360, Electro Industries). An IR camera (C2, FLIR) was used to ensure that the tendon was heating equally across its surface, and determine when the cTPE temperature had reached 75 °C. When the IR camera read a maximum temperature of 75 °C, the actual temperature of the cTPE was likely higher than the measured value because the silicone rubber acted as a thermal insulator; therefore, since any temperature above 72.9 °C was sufficient for melting, we could ensure the cTPE was in the active state. All measurements in the activated state were made at 75 °C, as measured by the IR camera, while measurements in the unactivated state were made at room temperature. Unless otherwise specified, all activation voltages were 5 V.

DSC (DSC Q20, TA Instruments) was performed on sample of cTPE (8.8 mg). Temperature was cycled between −80 and 150 °C, at a rate of 10 °C min^{-1} for four cycles.

The dynamic mechanical behavior of cTPE was evaluated using the tension mode on a Dynamic Mechanical Analyzer (Model 2980, TA Instruments). The samples were prepared with a dimension of 15.0 mm × 5.0 mm × 0.5 mm. The storage modulus was determined by straining the sample at a frequency of 1.0 Hz and amplitude of 50 µm. The temperature was increased from −40 to 80 °C at a heating rate of 3 °C min^{-1}.

The tendons were loaded on a universal testing machine (Model 5969, Instron) using 3D-printed clips. Both the top and bottom clips supported a screw that passed through the unactivated portion of the Ecoflex and cTPE, so tension could be applied directly to the tendon.

To calculate the modulus in both the activated and unactivated state, each sample was repeatedly loaded between 0% and 2.5% strain at a rate of 0.5 mm s^{-1}. An effective modulus was calculated for each state by averaging the slope of the loading and unloading stress–strain curves.

The recoverability was tested by activating the tendon and deforming it to 10% strain. The new natural length was measured, and the test was repeated for increasing values of strain until the tendon failed. Failure was defined as the inability to heat to activation or the initiation of tearing in the sample. Although the tendon's activated state corresponded to the melt state of the cTPE, excessive strain could cause breakage in the tendon that could not be repaired without applying considerable pressure.

The activation time was measured by preloading each sample to 750 kPa, and applying a voltage between 5 and 20 V, while measuring the decline in stress as a function of time. The activation time was considered to be the time at which the sample's modulus had decreased 90% of its total drop. The participant who administered the rigidity tuning splint in the video S3 provided informed signed consent.

Supporting Information

Supporting Information is available from the Wiley Online Library or from the author.

Acknowledgements

The authors would like to thank Onder Erin, Tess Hellebrekers, and Dr. Guo Zhan Lum for their suggestions on the paper's language, and Dipanjan Saha and the members of the Integrated Soft Materials Lab at Carnegie Mellon University for their helpful discussions. This work was supported by the Samsung Global Research Outreach Program (Award #A019487; Technical Contact: Dr. Youngbo Shim).

Conflict of Interest

The authors declare no conflict of interest.

Keywords

conductive elastomer, EGaIn, rigidity tuning, soft robotics, stiffness tuning

Received: July 7, 2017
Revised: August 6, 2017
Published online:

[1] D. W. Jung, T. Blangé, H. de Graaf, B. W. Treijtel, *Biophys. J.* **1988**, *54*, 897.
[2] W. M. Kier, *J. Exp. Biol.* **2012**, *215*, 1247.
[3] T. Motokawa, *Biol. Rev.* **1984**, *59*, 255.
[4] M. Cianchetti, M. Manti, V. Cacucciolo, C. Laschi, *IEEE Rob. Autom. Mag.* **2016**, *23*, 93.
[5] C. S. Haines, M. D. Lima, N. Li, G. M. Spinks, J. Foroughi, J. D. Madden, S. H. J. Kim, S. Fang, M. J. de Andrade, F. Goktepe, O. Goktepe, S. M. Mirvakili, S. Naficy, X. Lepro, J. Oh, M. E. Kozlov, S. H. J. Kim, X. Xu, B. J. Swedlove, G. G. Wallace, R. H. Baughman, *Science* **2014**, *343*, 868.
[6] J. Wirekoh, Y.-L. Park, *Smart Mater. Struct.* **2017**, *26*, 035009.
[7] J. R. Capadona, K. Shanmuganathan, D. J. Tyler, S. J. Rowan, C. Weder, *Science* **2008**, *319*, 1370.
[8] E. Brown, N. Rodenberg, J. Amend, A. Mozeika, E. Steltz, M. R. Zakin, H. Lipson, H. M. Jaeger, *Proc. Natl. Acad. Sci. USA* **2010**, *107*, 18809.
[9] J. Ou, L. Yao, D. Tauber, J. Steimle, R. Niiyama, H. Ishii, in *Proc. of the 8th Int. Conf. on Tangible, Embedded and Embodied Interaction – TEI '14*, **2013**, p. 65.
[10] S. Diller, C. Majidi, S. H. Collins, in *Proc. of the IEEE Int. Conf. on Robotics and Automation*, **2016**, p. 682.
[11] K. Suzumori, S. Wakimoto, K. Miyoshi, K. Iwata, *IEEE Int. Conf. on Intelligent Robots and Systems*, **2013**, p. 4454.
[12] A. Stilli, H. A. Wurdemann, K. Althoefer, *IEEE Int. Conf. on Intelligent Robots and Systems*, **2014**, p. 2476.
[13] F. Carpi, G. Frediani, C. Gerboni, J. Gemignani, D. De Rossi, *Med. Eng. Phys.* **2014**, *36*, 205.
[14] Y. Shan, M. Philen, A. Lotfi, S. Li, C. E. Bakis, C. D. Rahn, K. W. Wang, *J. Intell. Mater. Syst. Struct.* **2008**, *20*, 443.
[15] W. Shan, S. Diller, A. Tutcuoglu, C. Majidi, *Smart Mater. Struct.* **2015**, *24*, 065001.
[16] A. Balasubramanian, M. Standish, C. J. Bettinger, *Adv. Funct. Mater.* **2014**, *24*, 4860.
[17] Z. Ye, G. Z. Lum, S. Song, S. Rich, M. Sitti, *Adv. Mater.* **2016**, *28*, 5087.
[18] G. Mcknight, R. Doty, A. Keefe, G. Herrera, C. Henry, *J. Intell. Mater. Syst. Struct.* **2010**, *21*, 1783.
[19] Y. Qiu, Z. Ren, W. Hu, C. Liu, Q. Pei, *SPIE Smart Structures and Materials+ Nondestructive Evaluation and Health Monitoring. International Society for Optics and Photonics* **2016**, *9798*, U-1.
[20] W. Shan, T. Lu, C. Majidi, *Smart Mater. Struct.* **2013**, *22*, 085005.
[21] A. Tonazzini, S. Mintchev, B. Schubert, B. Mazzolai, J. Shintake, D. Floreano, *Adv. Mater.* **2016**, *28*, 10142.
[22] I. M. Van Meerbeek, B. C. Mac Murray, J. W. Kim, S. S. Robinson, P. X. Zou, M. N. Silberstein, R. F. Shepherd, *Adv. Mater.* **2016**, *28*, 2653.
[23] Y. Yang, Y. Chen, Y. Li, Z. Wang, Y. Li, *Soft Rob.* **2017**, *00*, https://doi.org/10.1089/soro.2016.0060.
[24] Y. Yang, Y. Chen, Y. Li, M. Z. Q. Chen, Y. Wei, *Soft Rob.* **2017**, *4*, 147.
[25] T. P. Chenal, J. C. Case, J. Paik, R. K. Kramer, *Intelligent Robots and Systems (IROS 2014). 2014 IEEE/RSJ International Conference*, IEEE, **2014**, pp. 2827–2831.
[26] B. E. Schubert, D. Floreano, *RSC Adv.* **2013**, *3*, 24671.
[27] L. Zheng, S. Yoshida, Y. Morimoto, H. Onoe, S. Takeuchi, *IEEE Int. Conf. Micro Electro Mech. Syst., 28th* **2015**, 18.
[28] C. Majidi, R. J. Wood, *Appl. Phys. Lett.* **2010**, *97*, 164104.
[29] L. Jiang, K. Low, J. Costa, R. J. Black, Y. L. Park, *IEEE Int. Conf. on Intelligent Robots and Systems*, **2015**, p. 1763.
[30] S. H. Jeong, K. Hjort, Z. Wu, *Sci. Rep.* **2015**, *5*, 8419.
[31] S. Kim, M. Sitti, T. Xie, X. Xiao, *Soft Matter* **2009**, *5*, 3689.
[32] N. Lazarus, S. S. Bedair, C. Meyer, *IEEE Sens. J.* **2014**, 1551.
[33] J. G. Simmons, *J. Appl. Phys.* **1963**, *34*, 1793.
[34] R. Shanks, I. Kong, *Thermoplast. Elastomers* **2012**.
[35] M. Knite, V. Teteris, A. Kiploka, J. Kaupuzs, *Sens. Actuators, A* **2004**, *110*, 142.
[36] J. C. Landsman, W. H. Seitz, A. I. Froimson, R. B. Leb, E. J. Bachner, *Orthopedics* **1995**, *18*, 1161.
[37] T. J. Baumgartner, D. R. Baumgartner, *U.S. Patent No. 7597671*, **2009**.